

# Inclusive photon production at forward rapidities in proton–proton collisions at $\sqrt{s} = 0.9, 2.76$ and 7 TeV

ALICE Collaboration\*

CERN, 1211 Geneva 23, Switzerland

Received: 19 November 2014 / Accepted: 11 March 2015 / Published online: 9 April 2015

© CERN for the benefit of the ALICE collaboration 2015. This article is published with open access at Springerlink.com

**Abstract** The multiplicity and pseudorapidity distributions of inclusive photons have been measured at forward rapidities ( $2.3 < \eta < 3.9$ ) in proton–proton collisions at three center-of-mass energies,  $\sqrt{s} = 0.9, 2.76$  and 7 TeV using the ALICE detector. It is observed that the increase in the average photon multiplicity as a function of beam energy is compatible with both a logarithmic and a power-law dependence. The relative increase in average photon multiplicity produced in inelastic pp collisions at 2.76 and 7 TeV center-of-mass energies with respect to 0.9 TeV are  $37.2 \pm 0.3\%$  (stat)  $\pm 8.8\%$  (sys) and  $61.2 \pm 0.3\%$  (stat)  $\pm 7.6\%$  (sys), respectively. The photon multiplicity distributions for all center-of-mass energies are well described by negative binomial distributions. The multiplicity distributions are also presented in terms of KNO variables. The results are compared to model predictions, which are found in general to underestimate the data at large photon multiplicities, in particular at the highest center-of-mass energy. Limiting fragmentation behavior of photons has been explored with the data, but is not observed in the measured pseudorapidity range.

## 1 Introduction

The large hadron collider (LHC) at CERN offers the possibility to study particle production mechanisms in proton–proton (pp) collisions at unprecedented center-of-mass energies. Measurements of multiplicity and pseudorapidity distributions of produced particles in pp collisions are important for the study of particle production mechanisms and to obtain the baseline distributions for heavy-ion collisions. Charged particle measurements in pp collisions at the LHC for central rapidities were reported by the ALICE [1,2], CMS [3] and ATLAS [4] collaborations and at forward rapidities by the LHCb collaboration [5,6]. Inclusive photon measurements provide complementary information to those of charged par-

ticles as the majority of the photons are decay products of neutral pions. Measurements at forward rapidities enable an extension of the study of particle production mechanisms carried out at mid-rapidities.

In the present work, we report the measurement of inclusive photon production in the forward pseudorapidity region,  $2.3 < \eta < 3.9$ , for pp collisions at  $\sqrt{s} = 0.9, 2.76$  and 7 TeV, with the ALICE detector. Multiplicity and spatial distribution of photons are measured on an event-by-event basis by the Photon Multiplicity Detector (PMD), which exploits the pre-shower photon measurement technique. We present the beam-energy dependence of the average photon multiplicity and pseudorapidity distributions of photons. The pseudorapidity distributions, plotted with respect to the corresponding beam rapidities, are used to test the predictions of the limiting fragmentation behavior [7]. The results are compared to different tunings of PYTHIA [8] and PHOJET [9,10] models.

This paper is organized as follows. Section 2 describes the experimental setup for the measurement of photons using the PMD. Event selection and trigger settings are discussed in Sect. 3. A discussion on the event generators and simulation framework is given in Sect. 4. Performance of the PMD modules for incident charged particle and electron beams are discussed in Sect. 5. Photon reconstruction is presented in Sect. 6 and the unfolding method used to correct for detector effects is described in Sect. 7. The study of the systematic uncertainties is outlined in Sect. 8. The results of photon multiplicities and pseudorapidity distributions are discussed in Sect. 9. We conclude with a summary and outlook in Sect. 10.

## 2 Experimental setup

The ALICE detector [11] consists of a large number of detector subsystems, and has a unique potential for pp physics in terms of excellent primary and secondary vertex reconstruction capabilities. The central barrel consists of the inner tracking system (ITS), the time projection chamber, the transition

\* e-mail: [alice-publications@cern.ch](mailto:alice-publications@cern.ch)

radiation detector, the time of flight detector and the electromagnetic calorimeter. The two silicon pixel detector (SPD) layers of the ITS surround the central beryllium beam pipe and cover the pseudorapidity ranges,  $|\eta| < 2$  and  $|\eta| < 1.4$  for the inner and outer layers, respectively. The central barrel also includes a high momentum particle identification detector and a photon spectrometer. The muon spectrometer and the PMD are both located at forward rapidities, but on opposite sides of the nominal interaction point. The present analysis uses data from the PMD for photon reconstruction. Several sets of trigger and multiplicity detectors are placed at forward rapidities, which include the forward multiplicity detector, the zero degree calorimeter and detectors for trigger and timing (V0 and T0). The V0 detector consists of two scintillator arrays, placed on either side of the interaction region, at  $2.7 < \eta < 5.1$  and  $-3.7 < \eta < -1.7$ . It is used for event selection and background rejection. The minimum bias (MB) trigger conditions are achieved by a combination of signals from V0 and SPD.

The PMD [12, 13] is located at a distance of 367 cm from the interaction point and spans a pseudorapidity region between 2.3 and 3.9, with full azimuthal coverage. The PMD makes use of the pre-shower technique where a three radiation length ( $X_0$ ) thick lead converter is sandwiched between two planes of highly granular gas proportional counters. The granularity and the converter thickness of the PMD are optimized for high particle density. The PMD consists of 184,320 honeycomb shaped gas cells arranged in 40 modules in the two planes. Each cell is of  $0.22 \text{ cm}^2$  area, and has a honeycomb shaped cathode extended towards a  $20 \text{ }\mu\text{m}$  thick gold-plated tungsten wire at ground potential at the center of each cell. The sensitive medium is a gas mixture of Ar and  $\text{CO}_2$  in a 70:30 ratio. The front-end electronics consists of MANAS chips for anode signal processing and the cluster read out concentrator unit system (CROCUS) for data acquisition [13]. The PMD is assembled in two equal halves. Each half has independent cooling, gas supply and electronics accessories. A photon traversing the converter plate produces an electromagnetic shower in the pre-shower plane, leading to a large signal, spread over several cells. The signal from a charged particle, on the other hand, is confined mostly to a single cell. The differences in the responses of charged particles to photons are used to reject charged tracks in the analysis.

### 3 Event selection

The data used in this analysis are from pp collisions at center-of-mass energies of 0.9, 2.76 and 7 TeV, collected by the ALICE detector with a magnetic field of 0.5 T. The number of analyzed events are 2, 8 and 9 millions at  $\sqrt{s} = 0.9, 2.76$  and 7 TeV, respectively. Data were taken in 2010 and 2011 under conditions where pileup effects were small. The prob-

**Table 1** The minimum bias trigger efficiency and the vertex reconstruction efficiency for pp collisions

$\sqrt{s}$ (TeV)	MB <sub>OR</sub> trigger efficiency (%)	Vertex reconstruction efficiency (%)
0.9	$91.0^{+3.2}_{-1.0}$	$91.4 \pm 1.7$
2.76	$88.1^{+5.9}_{-3.5}$	$92.4 \pm 1.1$
7.0	$85.2^{+6.2}_{-3.0}$	$92.8 \pm 1.2$

ability of collision pileup per triggered event was below 3%. Events with more than one vertex reconstructed with the SPD was rejected to minimize the effect of pileup. This rejection is especially effective at rejecting average and high multiplicity pileup events which can contaminate the multiplicity distribution.

The interaction vertex is reconstructed using the two silicon pixel layers of the SPD. For the present analysis, we restrict the measured  $z$ -vertex to be within  $\pm 10$  cm from the nominal interaction point. The minimum bias data used for the inelastic (INEL) events were collected using a minimum bias trigger (MB<sub>OR</sub>) condition, which requires at least one hit in the SPD or in either of the two V0 arrays [1]. This condition is satisfied by the passage of a charged particle anywhere in the 8 units of pseudorapidity covered by these detectors. The analysis for non-single diffractive (NSD) events requires a coincidence between the two sides of the V0 detectors. Except for the trigger selection criteria, identical data analyses procedures were followed for both INEL and NSD events. The experimental results are corrected for trigger and vertex reconstruction efficiencies, estimated by means of Monte Carlo (MC) simulations [14]. Table 1 lists the two efficiencies. The systematic errors due to these efficiencies affect the zero multiplicity bin, but are negligible for other multiplicity bins. For the zero bins, these systematic errors are 18, 29.3 and 26.7% for the data at 0.9, 2.76 and 7 TeV, respectively. Multiplicity-dependent correction factors are used to obtain the photon multiplicity distributions, whereas an overall correction factor is applied for pseudorapidity densities of photons.

### 4 Event generators and simulation framework

Corrections for the instrumental effects in the photon measurement and the estimation of systematic uncertainties are performed based on simulated events using various tunes of PYTHIA and PHOJET event generators. The PYTHIA event generator combines perturbative QCD and phenomenologically motivated models. PYTHIA employs several tunable parameters, which result in different tunes of the event generator, such as PYTHIA 6.4 [8] tune D6T [15], Perugia-0 [16], and ATLAS-CSC [17]). The PHOJET 1.2 generator [9, 10]

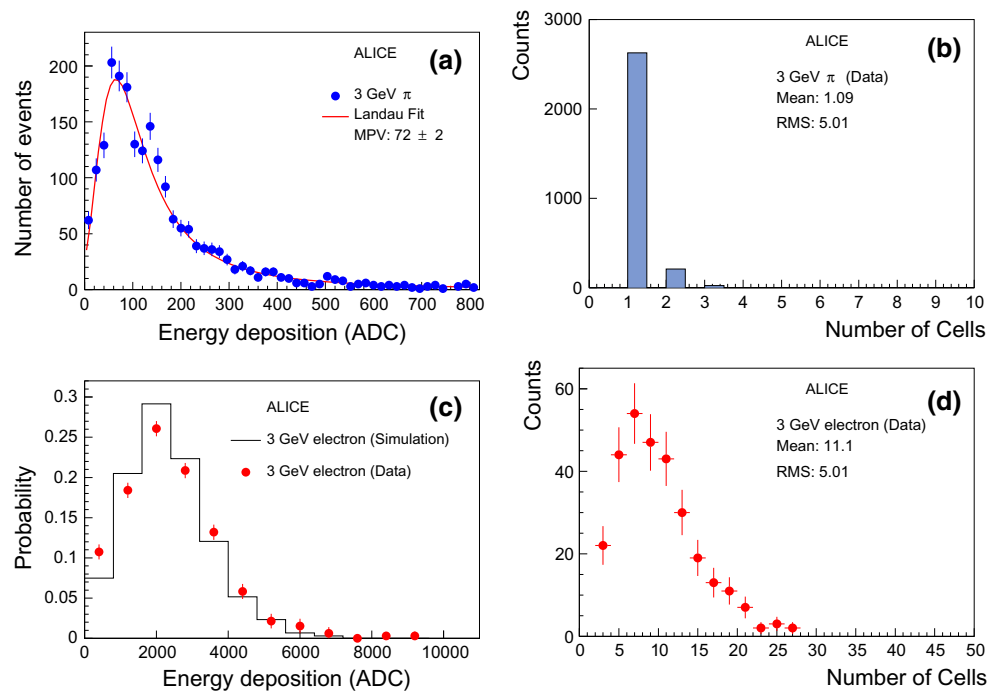


**Fig. 1** **a, c** The energy depositions in the PMD module for 3 GeV pions and 3 GeV electrons, respectively. The pion distribution is fitted with a Landau fit, which gives the most probable value (MPV) of energy depositions by charged particles. For electrons, the result from the sim-

ulation is superimposed on the experimental data. **b, d** The number of cells hit for 3 GeV pions and 3 GeV electrons, respectively. Note the large difference in scales in the abscissa for pions and electrons

is based on a two-component approach, that describes high-energy collisions as an interplay of soft and hard components.

The response of the PMD to the produced particles is studied using PYTHIA and PHOJET event generators. The AliRoot [18] software package, which includes a detailed information of ALICE apparatus, has been utilized. Particle transport of the generated particles from the event generators have been simulated using the GEANT-3 [19] software package, and stored in terms of energy depositions and positions of the hits. The deposited energy is converted to ADC values using the energy loss conversion relation to treat the simulated data on a similar footing as the experimental data. The MC description of the cluster sizes has been validated using test beam data. The distribution of cluster sizes for photon candidates was found to reproduce well the measured distribution, even in the tail region.

## 5 Performance of the PMD

The performance of the PMD has been studied by exposing the detector modules to pion and electron beams at energies ranging from 1 to 6 GeV at the CERN Proton Synchrotron. Two modules were mounted back to back on a movable stand. A gap was maintained between the modules to place different thickness of lead converters for the pre-

shower study. Data were readout by using same front-end electronics and data acquisition as in the real experiment. Special trigger combinations, using scintillator paddles and Cherenkov counters, were configured for pion and electron beams separately. Data were collected for various combinations of beam energy, converter thickness and detector operating voltage. The responses of the modules to pion and electron beams have been simulated by using GEANT-3 code, to understand the observed data.

Results for the performance of the PMD modules are presented in Fig. 1 for an operating voltage of  $-1300$  V. Energy deposition (in terms of ADC) and number of cells hit for 3 GeV pions are shown in the top panels of the figure. The most probable value (MPV) of the energy deposition by charged particles is obtained by fitting to a Landau distribution function, which yields an ADC value of  $72 \pm 2$ . This MPV value is used later in the manuscript to discriminate charged particle contamination in the photon sample. Pre-shower characteristics were studied by placing the lead converter and by bombarding the detector with electron beams of different energies. The bottom panels of the figure show the response of the module to 3 GeV electron beams for a  $3X_0$  converter thickness. The mean energy deposition of  $\sim 2000$  ADC is much larger than that of the response of the pions. It has also been observed that the signals from a charged hadrons affect on average  $\sim 1.1$  cells, whereas signals from 3 GeV elec-

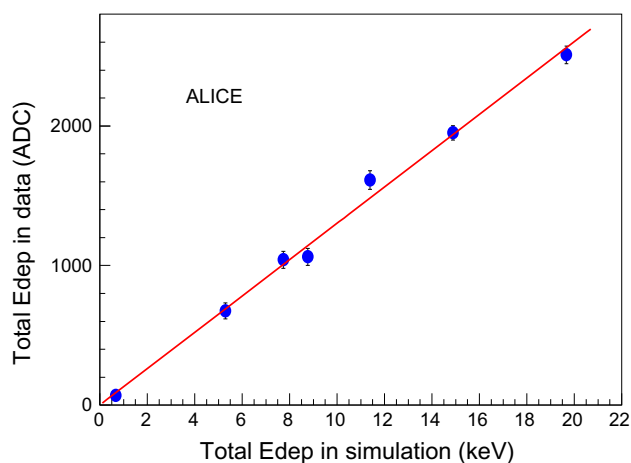


**Fig. 2** Relationship between the mean energy depositions in the PMD modules obtained from simulated results (in keV) and experimental data (in ADC) for pion and electron beams of various energies

trons affect 11 cells. Thus, compared to the charged pions, the electrons deposit larger amounts of energies and affect larger number of cells.

Mean energy depositions in the detector modules have been obtained from both experimental data and simulations. Figure 2 shows the relationship between the mean energy depositions, obtained from the simulated data (in keV) and the experimental data (in ADC) for pion and electron beams of different energies. A linear fit gives the conversion relation from the simulated to experimental data. This relation has been used in the analysis chain to convert the keV scale of the simulated data to total ADC of the experimental data.

During the data taking period at the LHC, all the modules of PMD are operated at  $-1300$  V, where the efficiency for charged pions is  $\sim 90\%$ . Responses of the cells to minimum bias particles have been obtained by storing single isolated clusters from the pp collisions at 7 TeV. Comparison of the MPV values for the cells give the cell-to-cell gain variation. For the full detector, the cell to cell gain variation is observed to be within 9%.

## 6 Photon reconstruction

Particles entering the pre-shower plane of the PMD are expected to affect more than one cell in general. To analyse the data, the cell hits were first clustered using a nearest neighbor clustering algorithm. Thus a cluster is formed by a number of contiguous cells having non-zero energy deposition. For each event, total number of clusters are obtained with corresponding cluster parameters, such as, number of hit cells in a cluster, position of the centroid of each cluster and the total energy deposition of the cluster.

To enrich the photon samples in the data, suitable photon-hadron discrimination thresholds on the number of hit cells and on the energy deposited in clusters, have been applied.

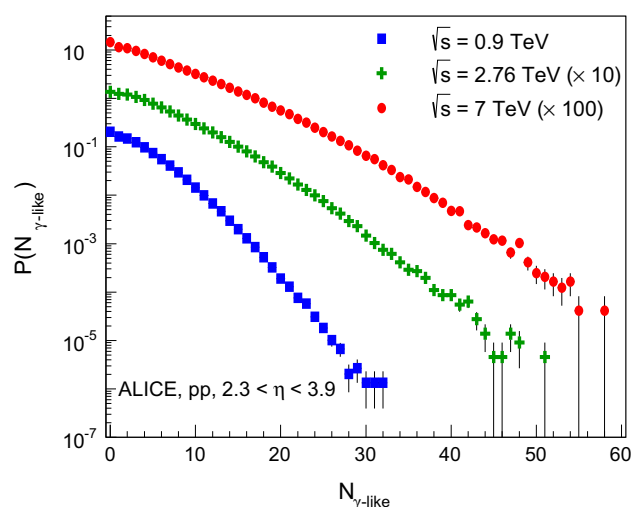


**Fig. 3** Probability distribution of the measured  $N_{\gamma\text{-like}}$  clusters (number of clusters above the photon-hadron discrimination thresholds) in pp collisions at  $\sqrt{s} = 0.9, 2.76$  and 7 TeV

The number of clusters in an event which pass through the threshold cuts are labelled as photon-like clusters,  $N_{\gamma\text{-like}}$ . Figure 3 shows the distributions of the number of  $N_{\gamma\text{-like}}$  clusters for the three energies within the detector acceptance of  $2.3 < \eta < 3.9$ , obtained with the application of discrimination thresholds, the number of cells greater than 2 and energy deposition greater than 9 times the MPV.

## 7 Correction for detector effects: method of unfolding

The material budget affects the photons originating at the vertex and travelling to the PMD. Photons and charged particles suffer from rescattering effects in upstream material and may interact with the detector material to produce secondary particles. The  $N_{\gamma\text{-like}}$  clusters are photon-rich clusters with a contamination of charged particles and secondaries which pass the threshold cut. The effects associated with finite detector acceptance and finite efficiency needs to be taken into account in the photon counting. These effects are handled by using detailed simulation and applying unfolding procedures.

The detector effects are modeled using a response function matrix ( $R_{mt}$ ). The matrix elements  $R_{mt}$  represent the conditional probability of measuring a true multiplicity  $t$  as a measured multiplicity  $m$ . The measured distribution,  $M$ , can thus be expressed as the product of response matrix and the true distribution  $T$ ,

$$M = R_{mt} T. \quad (1)$$

One can therefore obtain the true distribution  $T$  for given  $M$ :

$$T = R_{mt}^{-1} M. \quad (2)$$

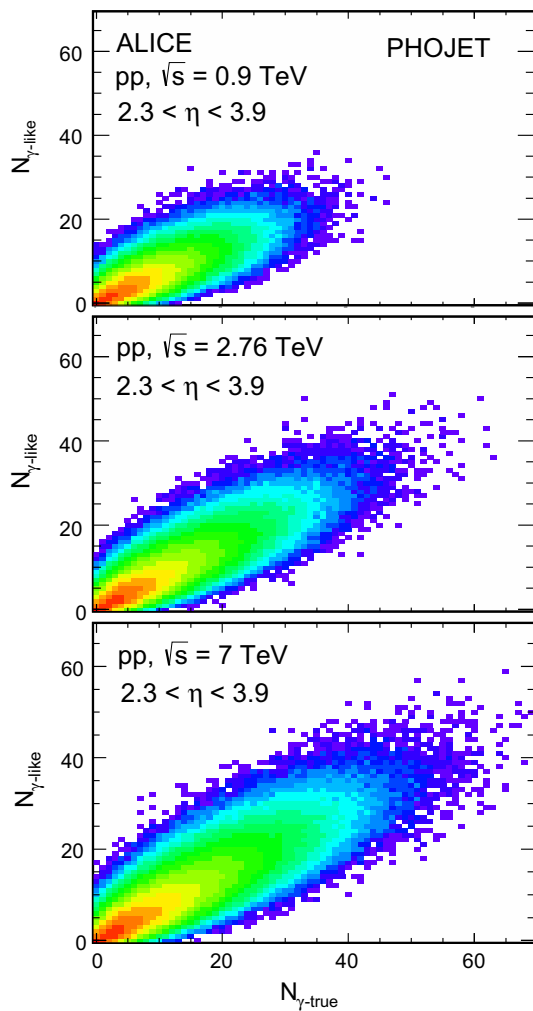


**Fig. 4** Detector response matrices in pp collisions at  $\sqrt{s} = 0.9, 2.76$  and  $7$  TeV using PHOJET event generator.  $N_{\gamma\text{-like}}$  and  $N_{\gamma\text{-true}}$  denote the measured and true photon multiplicities, respectively

However the matrix,  $R$ , may be singular and can not always be inverted analytically. Furthermore, even if the exact solution exists, it oscillates due to finite statistics in the measured distribution. A regularized unfolding method based on  $\chi^2$  minimization is used to overcome this problem [1, 20, 21].

The unfolded multiplicity distribution,  $U(N_\gamma)$ , is found by minimizing the  $\chi^2$  function, which is defined as:

$$\hat{\chi}^2(U) = \sum_m \left( \frac{M_m - \sum_t R_{mt} U_t}{e_m} \right)^2 + \beta P(u), \quad (3)$$

where  $e_m$  is the estimated measurement error,  $P(u)$  is the regularization term and  $\beta$  is the regularization coefficient.  $\beta P(u)$  suppresses high frequency components in the solution.

Figure 4 shows the response matrices, constructed using the PHOJET event generator within  $2.3 < \eta < 3.9$  in pp collisions at  $\sqrt{s} = 0.9, 2.76$  and  $7$  TeV. They represent the corre-

lation between the true photon multiplicity ( $N_{\gamma\text{-true}}$ ) of incident photons and the measured photon multiplicity ( $N_{\gamma\text{-like}}$ ) obtained after applying the photon-hadron discrimination criteria on the reconstructed clusters. It was found in MC studies that to unfold the full multiplicity distribution with good precision two different  $\beta$  values were needed, one for the two lowest multiplicity (0 and 1) bins and the second one for all other multiplicities. The performance of the unfolding method has been tested using simulated data of pp collisions at  $\sqrt{s} = 0.9, 2.76$  and  $7$  TeV as shown in Fig. 5. The ratios of the unfolded to true multiplicity distributions agree within 10% except for the highest multiplicities. Sensitivity of the results were verified by using different regularization functions, with various  $\beta$  values.

An alternate method of unfolding based on Bayes' theorem [22] has also been used, which describes the definite relationship between the probability of an event with  $m$  measured particles conditional on another event with  $t$  true multiplicity. This results in:

$$\bar{R}_{tm} = \frac{R_{mt} P_t}{\sum_{t'} R_{mt'} P_{t'}}, \quad (4)$$

where  $R$  is the response matrix and  $P_t$  is the apriori distribution of the true spectrum. After obtaining  $\bar{R}_{tm}$ , the unfolded distribution ( $U$ ) can be obtained as:

$$U_t = \sum_m \bar{R}_{tm} M_m. \quad (5)$$

The resultant  $U_t$  of an iteration is used as the new a priori distribution for the next iteration.

After unfolding, the results are corrected for trigger and vertex reconstruction efficiencies to obtain the final results. The above procedure is used to obtain the photon multiplicity. To obtain the pseudorapidity distribution of photons, the unfolding method has been employed separately in eight  $\eta$  bins of width 0.2.

### 8 Systematic uncertainties

The systematic uncertainties on the photon multiplicity have contributions from several effects. A major source for the systematic uncertainty to photon counting comes from the uncertainty in the implementation of all the known material between the vertex and the PMD in AliRoot. The material budget at forward rapidities was intensely studied in connection with the charged particle multiplicity measurements in Pb-Pb collisions [23]. Special sub-sample of events, where the vertex was displaced between  $-187.5$  cm to  $375$  cm, so that the material budget in front of the FMD and V0 detectors was almost negligible, was used to benchmark the MC description of the detector material. Discrepancies of the order of 6% were found in the same rapidity region

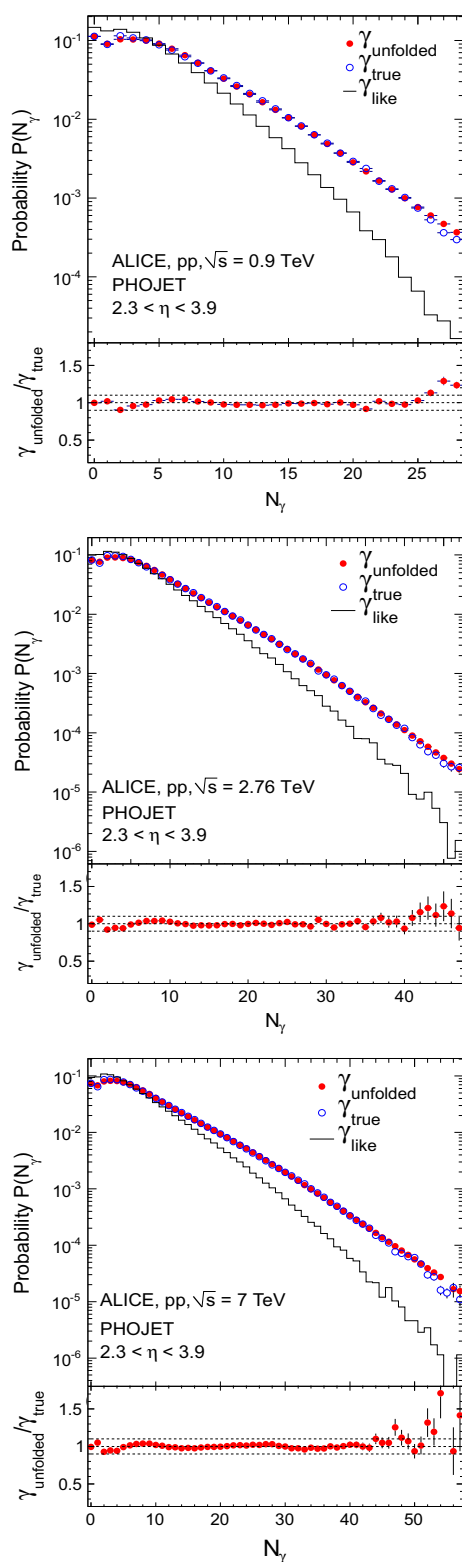


**Fig. 5** Test of the unfolding method using PHOJET event generator for pp collisions at  $\sqrt{s} = 0.9$  (top), 2.76 (middle) and 7 TeV (bottom). The measured, unfolded and true photon multiplicities are presented. The lower panels show the ratios of unfolded to true multiplicity distributions

covered by the PMD. Based on this study, a conservative uncertainty on the material budget of 10% has been used in the analysis. Events with default material description and with the 10% increase in material have been simulated. The response matrix, using the PHOJET event generator, is obtained from the default material setting and the unfolding procedure is followed for both the default material setting and with 10% increase of material. The difference between the two unfolded multiplicities is quoted as the systematic uncertainty to the multiplicity distribution of photons. The same procedure has been adopted for each  $\eta$  bin to obtain the systematic uncertainties for pseudorapidity distributions of photons.

The sensitiveness of the PMD to incident photons of different momenta depends primarily on the conversion efficiency of photons in the detector and then on the discrimination criteria. Simulation studies have shown that the detector is sensitive to transverse momenta as low as  $\sim 50$  MeV. The photon multiplicity is extracted after the unfolding method, where incident photons of all energy are considered, which makes the present photon measurement inclusive. Systematic uncertainties arising because of the choice of discrimination threshold and event generators need to be considered for the photon counting.

The photon-hadron discrimination conditions in terms of number of cells hit and energy depositions were optimized to minimize the contamination from charged particles and secondaries. The purity of the photon sample with the default discrimination condition (number of cells greater than 2 and energy deposition greater than 9 times the MPV) is 65%, which is consistent with the design value [12, 13]. The uncertainty due to the choice of the thresholds have been obtained by changing the discrimination conditions, that is, the number of cells greater than 2 and energy depositions greater than 6 times MPV. In this condition, the purity of the photon sample reduces to 60%. Photon counting is also affected by the non-uniformity in the PMD, which is taken care of by obtaining the cell-to-cell gain variation. Its effects on the photon multiplicity and pseudorapidity distributions have been included as a part of the systematic uncertainty.

The choice of the event generator may affect the photon counting. Two different generators, PHOJET and PYTHIA (tune D6T), have been used as a source of systematic uncertainty. The choice of the unfolding method may also add to the uncertainty. This is studied by using two different unfolding methods,  $\chi^2$  minimization and Bayesian methods. In addition, different regularization functions during the unfolding procedure also add to the systematic uncertainty.

Separate response matrices were generated to evaluate the systematic uncertainties for each of the sources, e.g., for PYTHIA and PHOJET. Although the contributions from these sources are calculated separately, most of the uncer-

**Table 2** Systematic uncertainties in the photon multiplicity for INEL collisions at three center-of-mass energies. The range of the errors corresponds to lowest and highest multiplicity values for each energy

Sources	0.9 TeV (%)	2.76 TeV (%)	7 TeV (%)
Material effect	3–18	3–18	3–18
Discrimination thresholds	0.4–4.1	4.3–6.7	0.1–1.6
Event generators	7.5–14.6	8.9–27.8	7.8–24.7
Unfolding methods	3.6–6.2	5.7–6.4	5.4–6.5
Regularization functions	4.1–9.5	1.9–9.6	3.0–10.7
Cell-to-cell gain variation	2.7	2.7	2.7
Total	10.1–26.4	12.4–35.8	10.8–33.2

**Table 3** The magnitude of the sources of systematic uncertainties and their contributions to the pseudorapidity distributions of photons for INEL collisions at each energy, spanning the range,  $2.3 < \eta < 3.9$

Source	0.9 TeV (%)	2.76 TeV (%)	7 TeV (%)
Material effect	7	7	7
Discrimination thresholds	1–2	1–2	1–2
Event generators	1–3	1–1.6	3–5
Unfolding methods	0–0.7	0–0.8	0–0.9
Regularization functions	0–0.6	0–0.8	0–0.4
Cell-to-cell gain variations	0.3	0.3	0.3
Total	7–7.9	7–7.5	8–8.6

tainties are likely to be correlated. The contributions from different sources of systematic uncertainties are quoted for photon multiplicity and pseudorapidity distributions of the photons in Tables 2 and 3, respectively. The total systematic uncertainties are obtained by adding in quadrature systematic uncertainties from the various sources.

### 9 Results and discussions

In this section, we present multiplicity and pseudorapidity distributions of photons within  $2.3 < \eta < 3.9$ . The results are compared to predictions from PHOJET and various tunes of PYTHIA.

#### 9.1 Multiplicity distributions

Figure 6 shows the multiplicity distributions of photons for inelastic pp collisions within  $2.3 < \eta < 3.9$  at  $\sqrt{s} = 0.9$  (top), 2.76 (middle) and 7 TeV (bottom). The statistical and systematic uncertainties of the data points are shown by the error bars and shaded bands, respectively. The average photon multiplicities for the collisions at 0.9 TeV are  $4.46 \pm 0.02$  (stat)  $\pm 0.20$  (sys), for 2.76 TeV collisions are  $6.12 \pm 0.01$  (stat)  $\pm 0.47$  (sys), and for 7 TeV collisions are  $7.19 \pm 0.01$  (stat)  $\pm 0.45$  (sys). The relative increase in average photon multiplicity for 2.76 and 7 TeV energies with respect to that

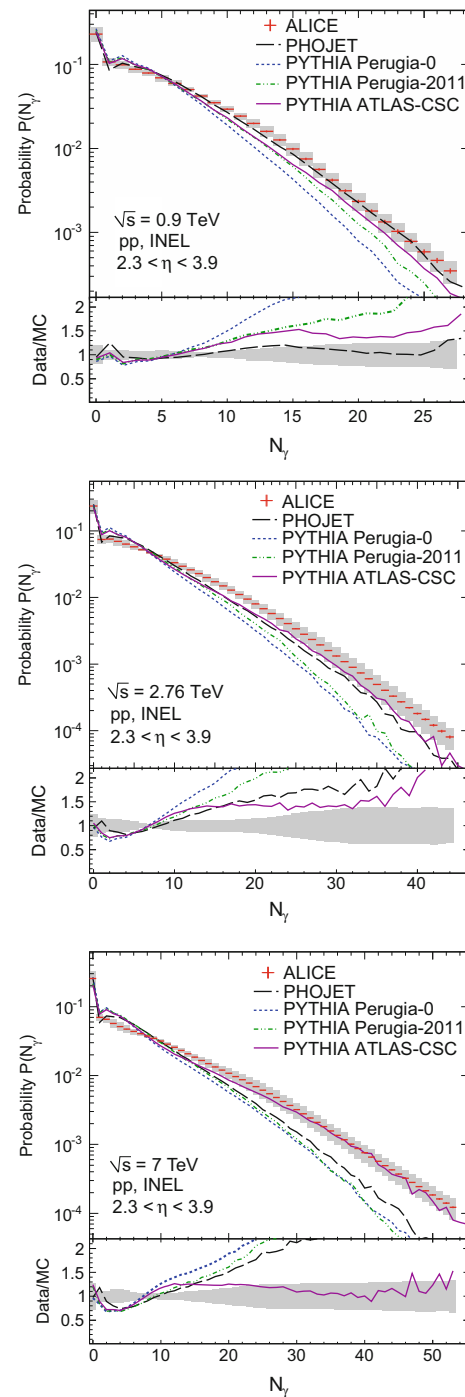


**Fig. 6** Multiplicity distributions of photons within  $2.3 < \eta < 3.9$  for inelastic events in pp collisions at  $\sqrt{s} = 0.9$  (top), 2.76 (middle) and 7 TeV (bottom). Predictions from different event generators are superimposed. Lower panels show the ratios between the data and MC distributions. The error bars are statistical and the shaded regions represent the systematic uncertainties

of the 0.9 TeV are  $37.2 \pm 0.3\%$  (stat)  $\pm 8.8\%$  (sys) and  $61.2 \pm 0.3\%$  (stat)  $\pm 7.6\%$  (sys) for inelastic collisions.

The multiplicity distributions are compared to the photon multiplicities obtained from PHOJET, PYTHIA Perugia-

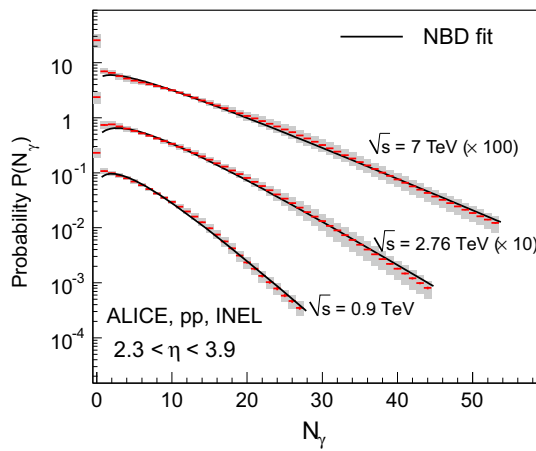


**Fig. 7** Multiplicity distribution of photons for inelastic collisions, fitted to single NBD functions for pp collisions at  $\sqrt{s} = 0.9, 2.76$  and  $7$  TeV. The error bars are statistical and the shaded regions represent the systematic uncertainties

**Table 4** Fit parameters of single NBD fitting to the photon multiplicity distribution

$\sqrt{s}$ in TeV	$k$	$\langle n \rangle$
0.9	$1.89 \pm 0.11$	$5.39 \pm 0.14$
2.76	$1.72 \pm 0.10$	$7.73 \pm 0.22$
7	$1.35 \pm 0.07$	$9.03 \pm 0.24$

0, PYTHIA Perugia-2011, and PYTHIA ATLAS-CSC. The bottom panel for each collision energy shows the ratios of experimental data to the event generators. PHOJET explains the data at 0.9 TeV, but overestimates the data at all other energies. Overall, the ATLAS-CSC tune of PYTHIA explains the data better at all the energies compared to other event generators. This is consistent with the charged particle multiplicity data at central rapidities [1,2].

Multiplicity distributions have traditionally been fitted by negative-binomial-distributions (NBD) to extract information regarding the nature of the particle production mechanism [24,25]. The photon multiplicity distributions are fitted with a NBD function of the form:

$$P(m, k; n) = \frac{\Gamma(n+k)}{\Gamma(n+1)\Gamma(k)} \frac{(m/k)^n}{(m/k+1)^{n+k}}, \quad (6)$$

where  $n$  is the photon multiplicity,  $m = \langle n \rangle$ ,  $k$  is a parameter responsible for shape of the distribution. The data, fitted with NBD function are shown in Fig. 7. The fitting is performed for  $N_\gamma > 0$ . Fits with the sum of two NBDs (not shown) do not significantly improve the description of the data. The parameters of the single NBD fit functions are reported in Table 4. With the increase of beam energy, the average photon multiplicity  $\langle n \rangle$  increases, whereas the values of  $k$ , related to dispersion of multiplicity, decrease.

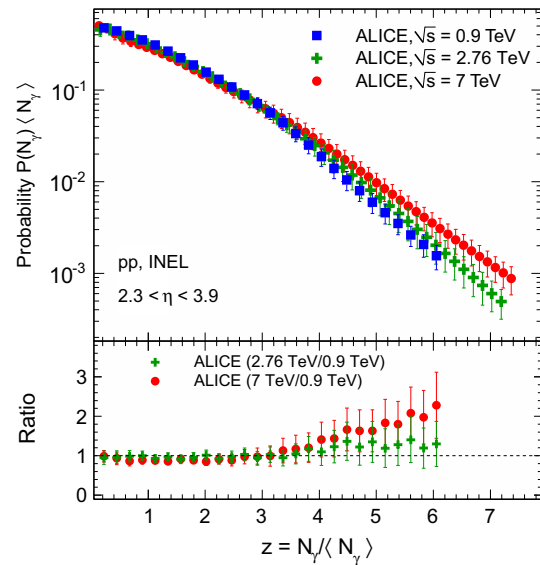


**Fig. 8** Upper panel shows the photon multiplicity distributions in terms of KNO variable for pp collisions at  $\sqrt{s} = 0.9, 2.76$  and  $7$  TeV for inelastic collisions. Lower panel shows the ratios of the distributions for 2.76 and 7 TeV with respect to 0.9 TeV

Scaling property of multiplicity distributions of produced particles had been proposed in 1972 by Koba, Nielsen and Olesen (KNO) [26], based on the assumption of Feynman scaling of particle production [27]. The multiplicity distributions, plotted in terms of the KNO variable,  $z = N_\gamma / \langle N_\gamma \rangle$ , are expected to be independent of collision energy [26,28]. To test this scaling at the forward rapidities at the LHC energies, the photon multiplicity distributions have been presented in terms of the KNO variable. The upper panel of Fig. 8 shows the distributions of  $z$  for the three energies,  $\sqrt{s} = 0.9, 2.76$  and  $7$  TeV. The distributions are similar for low values of  $z$ , while for higher  $z$  values ( $z > 3$ ), the three distributions deviate from each other. The deviations are studied by plotting the ratios of the  $z$  values for  $\sqrt{s} = 2.76$  and  $7$  TeV with respect to  $\sqrt{s} = 0.9$  TeV, shown in the lower panel of Fig. 8. Because of the difference in the  $z$  values, the nearest values of  $z$  are considered at other energies. The ratios are close to unity up to a value of  $z = 3$  and deviate from unity for  $z > 3$ . Although the error bars at high multiplicities are large, there is an indication of a mild deviation from the KNO scaling, similar to what has been observed for charged particles at mid-rapidity [1]. Violations of KNO scaling for charged particle multiplicities had been observed earlier for pp and  $p\bar{p}$  collisions at  $\sqrt{s} = 30$  GeV to 1800 GeV at the Fermilab Tevatron and also in UA5 experiment at CERN at 546 GeV [29–31]. The present observation at the LHC energies is consistent with these findings.

The energy dependences of the average photon multiplicity in INEL and NSD events within  $2.3 < \eta < 3.9$  are presented in Fig. 9. The NSD events are obtained using a



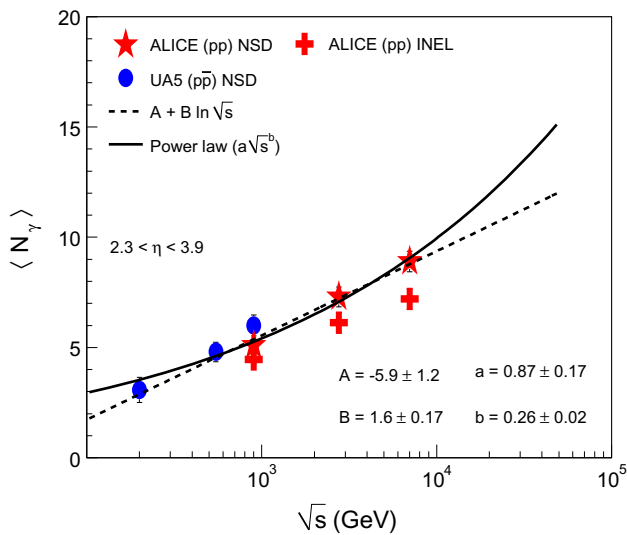


**Fig. 9** Average photon multiplicity within  $2.3 < \eta < 3.9$  as a function of center of mass energy for pp collisions. The data points from UA5 experiment [32] are superimposed on the ALICE data. The energy dependence for the NSD events is consistent with both a logarithmic and a power-law fit

special trigger condition as discussed in Sec. 3. At lower center of mass energies of 0.2, 0.546 and 0.9 TeV, the average photon multiplicities for NSD events have been measured by the UA5 experiment [32] within the same pseudorapidity region. It is seen that the average photon multiplicity increases with increasing  $\sqrt{s}$ . The nature of the increase has been studied in order to understand the particle production mechanism and for extrapolating to higher energy collisions. A logarithmic increase in average multiplicity with respect to  $\sqrt{s}$  has been predicted by the Feynman scaling of particle production [27,33]. For the NSD events, a logarithmic fit of the form  $A + B \ln \sqrt{s}$  yields  $A = -5.9 \pm 1.2$  and  $B = 1.6 \pm 0.17$ , where  $\sqrt{s}$  is expressed in GeV. On the other hand, phase space considerations give a power law dependence of particle multiplicity [34]. A power-law function of the form  $a(\sqrt{s})^b$  gives an equally good fit to the NSD data points with  $a = 0.87 \pm 0.17$  and  $b = 0.26 \pm 0.02$ . Thus, the present data cannot distinguish between the logarithmic and power law dependence on  $\sqrt{s}$ . At higher energies, the power-law fit predicts somewhat larger photon multiplicity compared to the logarithmic function. Data points at higher energies are needed to draw a conclusion on the nature of the increase of photon multiplicity, and in this context future LHC runs will be useful.

### 9.2 Pseudorapidity distributions and limiting fragmentation

Pseudorapidity distributions of photons for the INEL collisions have been obtained after applying the unfolding method in each  $\eta$  bin. In Fig. 10, the results for pseudorapidity

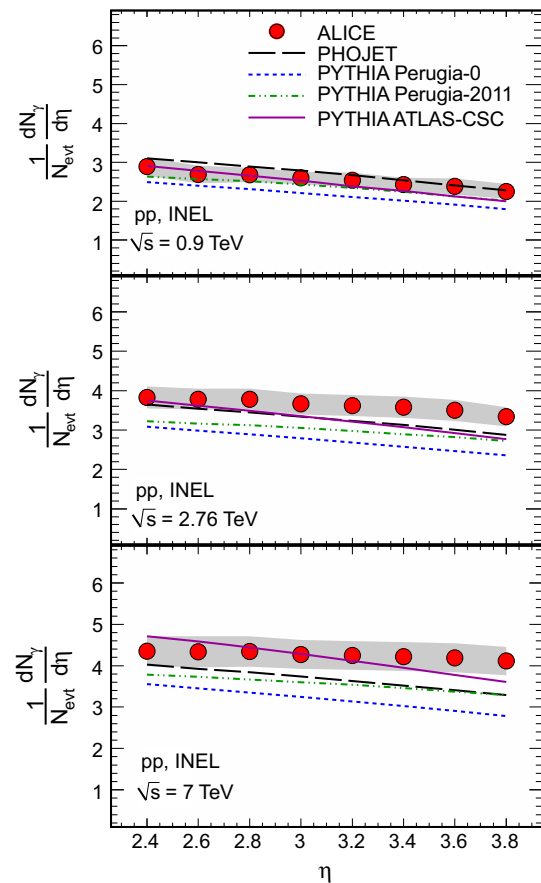


**Fig. 10** Pseudorapidity distribution of photons for inelastic events for pp collisions at  $\sqrt{s} = 0.9$  (top), 2.76 (middle) and 7 TeV (bottom). Results from different event generators are superimposed. The statistical errors are within the symbol sizes and the shaded regions represent the systematic uncertainties

density are plotted as a function of pseudorapidity. Results from PHOJET 1.2 and three different tunes of PYTHIA 6.4 event generators are superimposed on the data points. At  $\sqrt{s} = 0.9$  TeV, all the calculations except PYTHIA (tune Perugia-0) describe the data within uncertainties, whereas at  $\sqrt{s} = 2.76$  TeV, PHOJET and PYTHIA (tune ATLAS-CSC) show a better agreement compared to other event generators. At  $\sqrt{s} = 7$  TeV, PYTHIA (tune ATLAS-CSC) are close to the data points, whereas all other calculations under-predict the data. Thus PYTHIA (tune ATLAS-CSC) results on the pseudorapidity distributions are the most compatible with the measured data points, within the present uncertainties.

Particle productions at forward rapidity in pp and in heavy-ion collisions are expected to follow the limiting fragmentation behavior. This means that particle production in the rest frame of one of the colliding hadrons is independent of center-of-mass energy [7,35,36]. This phenomenon is attributed to the longitudinal scaling of particle multiplicities. This behavior is studied by shifting the pseudorapidity bins by the beam rapidity,  $y_{\text{beam}}$ . The UA5 experiment at

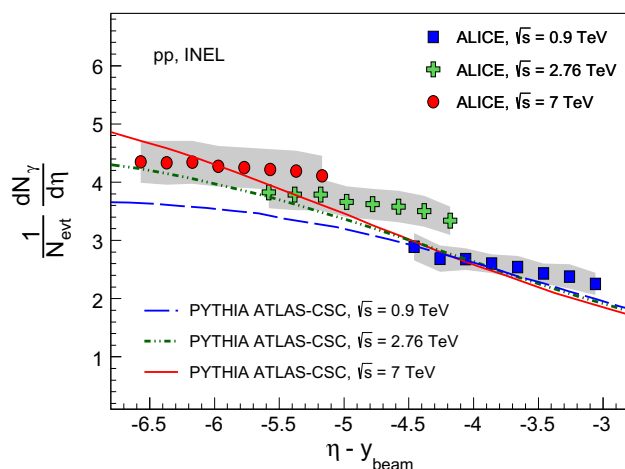


**Fig. 11** Pseudorapidity distribution of photons for inelastic events as a function of  $\eta - y_{\text{beam}}$  for pp collisions at  $\sqrt{s} = 0.9, 2.76$  and  $7$  TeV. Corresponding distributions from PYTHIA (tune ATLAS-CSC) are superimposed. The statistical uncertainties are within symbol sizes and the shaded regions represent the systematic uncertainties

CERN has observed the limiting fragmentation behavior in pp and  $p\bar{p}$  inelastic collisions from 53 GeV to 900 GeV [37] for charged particles in  $|\eta - y_{\text{beam}}| > -2.5$ . Such observations have also been made for nucleus-nucleus collisions at RHIC energies [38–40]. For the present analyses, the  $y_{\text{beam}}$  values are 6.86, 7.98 and 8.97 at  $\sqrt{s} = 0.9, 2.76$  and  $7$  TeV, respectively. The results of the pseudorapidity distributions of photons, after shifting for the beam rapidity, are presented in Fig. 11. The distributions from PYTHIA (tune ATLAS-CSC) event generator are also presented in Fig. 11 for all three energies, which indicate that the limiting fragmentation behavior of photons hold for  $|\eta - y_{\text{beam}}| < -4.5$ . In the range of the present measurement, limiting fragmentation behavior is not expected and not observed. This suggests that at the LHC this behavior may be confined to a pseudorapidity interval closer to beam rapidity.

## 10 Summary

We have measured the multiplicity and pseudorapidity distributions of photons in pp collisions at  $\sqrt{s} = 0.9, 2.76$  and  $7$  TeV in the forward rapidity region ( $2.3 < \eta < 3.9$ ) using the PMD installed in the ALICE detector. The results are compared to the photon multiplicity distributions obtained with different event generators. It is observed that PHOJET explains the multiplicity distributions at  $\sqrt{s} = 0.9$  TeV, but under-predicts the data at other energies. At  $\sqrt{s} = 2.76$  TeV and  $7$  TeV, the results from the ATLAS-CSC tune of PYTHIA are closer to the data compared to all other event generators. Photon multiplicity distributions are well described by single NBD functions. We observe deviations from KNO scaling for

$z > 3$ . The energy dependence of the average photon multiplicity within  $2.3 < \eta < 3.9$  increases with the increase in  $\sqrt{s}$ , and is consistent with both a logarithmic and a power-law dependence. The pseudorapidity distributions of photons have been presented and compared to the results from event generators. Results from PYTHIA (tune ATLAS-CSC) are most compatible with the measured data points compared to other generators. Longitudinal scaling of photon production is not observed within the measured pseudorapidity range. Future measurements at larger rapidities will help in better understanding of the limiting fragmentation behavior.

**Open Access** This article is distributed under the terms of the Creative Commons Attribution License which permits any use, distribution, and reproduction in any medium, provided the original author(s) and the source are credited.

Funded by SCOAP<sup>3</sup> / License Version CC BY 4.0.

## References

- ALICE Collaboration, K. Aamodt et al., Charged-particle multiplicity measurement in proton–proton collisions at  $\sqrt{s} = 0.9$  and  $2.36$  TeV with ALICE at LHC. *Eur. Phys. J. C* **68**, 89–108 (2010). [arXiv:1004.3034](#) [hep-ex]
- ALICE Collaboration, K. Aamodt et al., Charged-particle multiplicity measurement in proton–proton collisions at  $\sqrt{s} = 7$  TeV with ALICE at LHC. *Eur. Phys. J. C* **68**, 345–354 (2010). [arXiv:1004.3514](#) [hep-ex]
- C.M.S. Collaboration, V. Khachatryan et al., Transverse-momentum and pseudorapidity distributions of charged hadrons in pp collisions at  $\sqrt{s} = 7$  TeV. *Phys. Rev. Lett.* **105**, 022002 (2010). [arXiv:1005.3299](#) [hep-ex]
- ATLAS Collaboration, G. Aad et al., Charged-particle multiplicities in pp interactions at  $\sqrt{s} = 900$  GeV measured with the ATLAS detector at the LHC. *Phys. Lett. B* **688**, 21–42 (2010). [arXiv:1003.3124](#) [hep-ex]
- LHCb Collaboration, R. Aaij et al., Measurement of charged particle multiplicities in pp collisions at  $\sqrt{s} = 7$  TeV in the forward region. *Eur. Phys. J. C* **72**, 1947 (2012). [arXiv:1112.4592](#) [hep-ex]
- LHCb Collaboration, R. Aaij et al., Measurement of charged particle multiplicities and densities in pp collisions at  $\sqrt{s} = 7$  TeV in the forward region. *Eur. Phys. J. C* **74**, 2888 (2014). [arXiv:1402.4430](#) [hep-ex]
- J. Benecke, T. Chou, C.-N. Yang, E. Yen, Hypothesis of limiting fragmentation in high-energy collisions. *Phys. Rev.* **188**, 2159–2169 (1969)
- T. Sjostrand, S. Mrenna, P.Z. Skands, PYTHIA 6.4 physics and manual. *JHEP* **0605**, 026 (2006). [arXiv:hep-ph/0603175](#) [hep-ph]
- R. Engel, Photoproduction within the two component dual parton model. 1. Amplitudes and cross-sections. *Z. Phys. C* **66**, 203–214 (1995)
- R. Engel, J. Ranft, S. Roesler, Hard diffraction in hadron hadron interactions and in photoproduction. *Phys. Rev. D* **52**, 1459–1468 (1995). [arXiv:hep-ph/9502319](#) [hep-ph]
- ALICE Collaboration, K. Aamodt et al., The ALICE experiment at the CERN LHC. *JINST* **3**, S08002 (2008)
- ALICE Collaboration, G. Dellacasa et al., ALICE technical design report: photon multiplicity detector (PMD). CERN-LHCC-99-32 (1999)

13. ALICE Collaboration, P. Cortese et al., ALICE: addendum to the technical design report of the photon multiplicity detector (PMD). CERN-LHCC-2003-038 (2003)
14. ALICE Collaboration, B. Abelev et al., Measurement of inelastic, single- and double-diffraction cross sections in proton–proton collisions at the LHC with ALICE. *Eur. Phys. J. C* **73**, 2456 (2013). [arXiv:1208.4968](#) [hep-ex]
15. M.G. Albrow et al., Tevatron-for-LHC report of the QCD working group. FERMILAB-CONF-06-359 (2006). [arXiv:hep-ph/0610012](#) [hep-ph]
16. P.Z. Skands, The Perugia tunes. FERMILAB-CONF-09-113-T, 284–297 (2009). [arXiv:0905.3418](#) [hep-ph]
17. ATLAS Collaboration, A. Moraes et al., ATLAS CSC (306) tune. ATLAS Note ATL-COM-PHYS-2009-119 (2009)
18. R. Brun, P. Buncic, F. Carminati, A. Morsch, F. Rademakers et al., Computing in ALICE. *Nucl. Instrum. Meth. A* **502**, 339–346 (2003)
19. R. Brun, F. Carminati, S. Giani, GEANT detector description and simulation tool. CERN-W5013, CERN-W-5013 (1994)
20. V. Blobel, An unfolding method for high-energy physics experiments. DESY-02-078, 258–267 (2002). [arXiv:hep-ex/0208022](#) [hep-ex]
21. J.F. Grosse-Oetringhaus, Measurement of the charged-particle multiplicity in proton–proton collisions with the ALICE detector. CERN-THESIS-2009-033. [urn:nbn:de:hbz:6-11589544049](#)
22. G. D’Agostini, A multidimensional unfolding method based on Bayes’ theorem. *Nucl. Instrum. Meth. A* **362**, 487–498 (1995)
23. ALICE Collaboration, E. Abbas et al., Centrality dependence of the pseudorapidity density distribution for charged particles in Pb–Pb collisions at  $\sqrt{s_{NN}} = 2.76$  TeV. *Phys. Lett. B* **726**, 610–622 (2013). [arXiv:1304.0347](#) [nucl-ex]
24. C. Fuglesang, UA5 multiplicity distributions and fits of various functions. CERN-EP-89-135, C89-03-20.3 (1989)
25. P. Ghosh, Negative binomial multiplicity distribution in proton–proton collisions in limited pseudorapidity intervals at LHC up to  $\sqrt{s} = 7$  TeV and the clan model. *Phys. Rev. D* **85**, 054017 (2012). [arXiv:1202.4221](#) [hep-ph]
26. Z. Koba, H.B. Nielsen, P. Olesen, Scaling of multiplicity distributions in high-energy hadron collisions. *Nucl. Phys. B* **40**, 317–334 (1972)
27. R.P. Feynman, Very high-energy collisions of hadrons. *Phys. Rev. Lett.* **23**, 1415–1417 (1969)
28. W.D. Walker, Multiparton interactions and hadron structure. *Phys. Rev. D* **69**, 034007 (2004)
29. T. Alexopoulos, E. Anderson, N. Biswas, A. Bujak, D. Carmony et al., The role of double parton collisions in soft hadron interactions. *Phys. Lett. B* **435**, 453–457 (1998)
30. UA5 Collaboration, R. Ansorge et al., Charged particle multiplicity distributions at 200-GeV and 900-GeV center-of-mass energy. *Z. Phys. C* **43**, 357 (1989)
31. S. Hegyia, KNO scaling 30 years later. *Nucl. Phys. Proc. Suppl.* **92**, 122 (2001)
32. UA5 Collaboration, R. Ansorge et al., Photon production at c.m. energies of 200-GeV and 900-GeV. *Z. Phys. C* **43**, 75–89 (1989)
33. J.F. Grosse-Oetringhaus, K. Reygers, Charged-particle multiplicity in proton–proton collisions. *J. Phys. G* **37**, 083001 (2010). [arXiv:0912.0023](#) [hep-ex]
34. E.L. Berger, A. Krzywicki, Kinematic aspects of inclusive phenomenology. *Phys. Lett. B* **36**, 380–384 (1971)
35. R. Beckmann, S. Raha, N. Stelte, R. Weiner, Limiting fragmentation in high-energy heavy ion reactions and preequilibrium. *Phys. Lett. B* **105**, 411 (1981)
36. F. Gelis, A.M. Stasto, R. Venugopalan, Limiting fragmentation in hadron–hadron collisions at high energies. *Eur. Phys. J. C* **48**, 489–500 (2006). [arXiv:hep-ph/0605087](#) [hep-ph]
37. UA5 Collaboration, G. Alner et al., Scaling of pseudorapidity distributions at c.m. energies up to 0.9-TeV. *Z. Phys. C* **33**, 1–6 (1986)
38. STAR Collaboration, J. Adams et al., Multiplicity and pseudorapidity distributions of charged particles and photons at forward pseudorapidity in Au + Au collisions at  $s(NN)^{1/2} = 62.4$ -GeV. *Phys. Rev. C* **73**, 034906 (2006). [arXiv:nucl-ex/0511026](#) [nucl-ex]
39. PHOBOS Collaboration, B. Back et al., Charged-particle pseudorapidity distributions in Au+Au collisions at  $s(NN)^{1/2} = 62.4$ -GeV. *Phys. Rev. C* **74**, 021901 (2006). [arXiv:0509034](#) [nucl-ex]
40. BRAHMS Collaboration, I. Bearden et al., Pseudorapidity distributions of charged particles from Au+Au collisions at the maximum RHIC energy. *Phys. Rev. Lett.* **88**, 202301 (2002). [arXiv:0112001](#) [nucl-ex]





N. Sharma<sup>120</sup>, S. Sharma<sup>86</sup>, K. Shigaki<sup>43</sup>, K. Shtejer<sup>9,25</sup>, Y. Sibiriak<sup>96</sup>, S. Siddhanta<sup>102</sup>, T. Siemiarczuk<sup>73</sup>, D. Silvermyr<sup>80</sup>, C. Silvestre<sup>67</sup>, G. Simatovic<sup>123</sup>, R. Singaraju<sup>126</sup>, R. Singh<sup>86</sup>, S. Singha<sup>75,126</sup>, V. Singhal<sup>126</sup>, B. C. Sinha<sup>126</sup>, T. Sinha<sup>97</sup>, B. Sitar<sup>36</sup>, M. Sitta<sup>30</sup>, T. B. Skaali<sup>21</sup>, K. Skjerdal<sup>17</sup>, M. Slupecki<sup>118</sup>, N. Smirnov<sup>131</sup>, R. J. M. Snellings<sup>53</sup>, C. Søggaard<sup>32</sup>, R. Soltz<sup>71</sup>, J. Song<sup>92</sup>, M. Song<sup>132</sup>, F. Soramel<sup>28</sup>, S. Sorensen<sup>120</sup>, M. Spacek<sup>37</sup>, E. Spiriti<sup>68</sup>, I. Sputowska<sup>112</sup>, M. Spyropoulou-Stassinaki<sup>84</sup>, B. K. Srivastava<sup>91</sup>, J. Stachel<sup>89</sup>, I. Stan<sup>58</sup>, G. Stefanek<sup>73</sup>, M. Steinpreis<sup>19</sup>, E. Stenlund<sup>32</sup>, G. Steyn<sup>61</sup>, J. H. Stiller<sup>89</sup>, D. Stocco<sup>109</sup>, M. Stolpovskiy<sup>108</sup>, P. Strmen<sup>36</sup>, A. A. P. Suaide<sup>115</sup>, T. Sugitate<sup>43</sup>, C. Suire<sup>47</sup>, M. Suleymanov<sup>15</sup>, R. Sultanov<sup>54</sup>, M. Šumbera<sup>79</sup>, T. J. M. Symons<sup>70</sup>, A. Szabo<sup>36</sup>, A. Szanto de Toledo<sup>115</sup>, I. Szarka<sup>36</sup>, A. Szczepankiewicz<sup>34</sup>, M. Szymanski<sup>128</sup>, J. Takahashi<sup>116</sup>, M. A. Tangaro<sup>31</sup>, J. D. Tapia Takaki<sup>47,h</sup>, A. Tarantola Peloni<sup>49</sup>, A. Tarazona Martinez<sup>34</sup>, M. Tariq<sup>18</sup>, M. G. Tarzila<sup>74</sup>, A. Tauro<sup>34</sup>, G. Tejada Muñoz<sup>2</sup>, A. Telesca<sup>34</sup>, K. Terasaki<sup>121</sup>, C. Terrevoli<sup>23</sup>, J. Thäder<sup>93</sup>, D. Thomas<sup>53</sup>, R. Tieulent<sup>124</sup>, A. R. Timmins<sup>117</sup>, A. Toia<sup>49,104</sup>, V. Trubnikov<sup>3</sup>, W. H. Trzaska<sup>118</sup>, T. Tsuji<sup>121</sup>, A. Tumkin<sup>95</sup>, R. Turrisi<sup>104</sup>, T. S. Tveter<sup>21</sup>, K. Ullaland<sup>17</sup>, A. Uras<sup>124</sup>, G. L. Usai<sup>23</sup>, M. Vajzer<sup>79</sup>, M. Vala<sup>55,62</sup>, L. Valencia Palomo<sup>66</sup>, S. Vallero<sup>25,89</sup>, P. Vande Vyvre<sup>34</sup>, J. Van Der Maarel<sup>53</sup>, J. W. Van Hoorne<sup>34</sup>, M. van Leeuwen<sup>53</sup>, A. Vargas<sup>2</sup>, M. Vargyas<sup>118</sup>, R. Varma<sup>44</sup>, M. Vasileiou<sup>84</sup>, A. Vasiliev<sup>96</sup>, V. Vechernin<sup>125</sup>, M. Veldhoen<sup>53</sup>, A. Velure<sup>17</sup>, M. Venaruzzo<sup>24,69</sup>, E. Vercellin<sup>25</sup>, S. Vergara Limón<sup>2</sup>, R. Vernet<sup>8</sup>, M. Verweij<sup>129</sup>, L. Vickovic<sup>111</sup>, G. Viesti<sup>28</sup>, J. Viinikainen<sup>118</sup>, Z. Vilakazi<sup>61</sup>, O. Villalobos Baillie<sup>98</sup>, A. Vinogradov<sup>96</sup>, L. Vinogradov<sup>125</sup>, Y. Vinogradov<sup>95</sup>, T. Virgili<sup>29</sup>, V. Vislavicius<sup>32</sup>, Y. P. Viyogi<sup>126</sup>, A. Vodopyanov<sup>62</sup>, M. A. Völkl<sup>89</sup>, K. Voloshin<sup>54</sup>, S. A. Voloshin<sup>129</sup>, G. Volpe<sup>34</sup>, B. von Haller<sup>34</sup>, I. Vorobyev<sup>125</sup>, D. Vranic<sup>34,93</sup>, J. Vrláková<sup>38</sup>, B. Vulpescu<sup>66</sup>, A. Vyushin<sup>95</sup>, B. Wagner<sup>17</sup>, J. Wagner<sup>93</sup>, V. Wagner<sup>37</sup>, M. Wang<sup>7,109</sup>, Y. Wang<sup>89</sup>, D. Watanabe<sup>122</sup>, M. Weber<sup>34,117</sup>, S. G. Weber<sup>93</sup>, J. P. Wessels<sup>50</sup>, U. Westerhoff<sup>50</sup>, J. Wiechula<sup>33</sup>, J. Wikne<sup>21</sup>, M. Wilde<sup>50</sup>, G. Wilk<sup>73</sup>, J. Wilkinson<sup>89</sup>, M. C. S. Williams<sup>101</sup>, B. Windelband<sup>89</sup>, M. Winn<sup>89</sup>, C. G. Yaldo<sup>129</sup>, Y. Yamaguchi<sup>121</sup>, H. Yang<sup>53</sup>, P. Yang<sup>7</sup>, S. Yang<sup>17</sup>, S. Yano<sup>43</sup>, S. Yasnopolskiy<sup>96</sup>, J. Yi<sup>92</sup>, Z. Yin<sup>7</sup>, I.-K. Yoo<sup>92</sup>, I. Yushmanov<sup>96</sup>, A. Zaborowska<sup>128</sup>, V. Zaccolo<sup>76</sup>, A. Zaman<sup>15</sup>, C. Zampolli<sup>101</sup>, S. Zaporozhets<sup>62</sup>, A. Zarochentsev<sup>125</sup>, P. Závada<sup>56</sup>, N. Zaviyalov<sup>95</sup>, H. Zbroszczyk<sup>128</sup>, I. S. Zgura<sup>58</sup>, M. Zhalov<sup>81</sup>, H. Zhang<sup>7</sup>, X. Zhang<sup>7,70</sup>, Y. Zhang<sup>7</sup>, C. Zhao<sup>21</sup>, N. Zhigareva<sup>54</sup>, D. Zhou<sup>7</sup>, F. Zhou<sup>7</sup>, Y. Zhou<sup>53</sup>, Zhou Zhuo<sup>17</sup>, H. Zhu<sup>7</sup>, J. Zhu<sup>7,109</sup>, X. Zhu<sup>7</sup>, A. Zichichi<sup>12,26</sup>, A. Zimmermann<sup>89</sup>, M. B. Zimmermann<sup>34,50</sup>, G. Zinovjev<sup>3</sup>, Y. Zoccarato<sup>124</sup>, M. Zyzak<sup>49</sup>

<sup>1</sup> A.I. Alikhanyan National Science Laboratory (Yerevan Physics Institute) Foundation, Yerevan, Armenia

<sup>2</sup> Benemérita Universidad Autónoma de Puebla, Puebla, Mexico

<sup>3</sup> Bogolyubov Institute for Theoretical Physics, Kiev, Ukraine

<sup>4</sup> Department of Physics and Centre for Astroparticle Physics and Space Science (CAPSS), Bose Institute, Kolkata, India

<sup>5</sup> Budker Institute for Nuclear Physics, Novosibirsk, Russia

<sup>6</sup> California Polytechnic State University, San Luis Obispo, CA, USA

<sup>7</sup> Central China Normal University, Wuhan, China

<sup>8</sup> Centre de Calcul de l'IN2P3, Villeurbanne, France

<sup>9</sup> Centro de Aplicaciones Tecnológicas y Desarrollo Nuclear (CEADEN), Havana, Cuba

<sup>10</sup> Centro de Investigaciones Energéticas Medioambientales y Tecnológicas (CIEMAT), Madrid, Spain

<sup>11</sup> Centro de Investigación y de Estudios Avanzados (CINVESTAV), Mexico City and Mérida, Mexico

<sup>12</sup> Centro Fermi-Museo Storico della Fisica e Centro Studi e Ricerche "Enrico Fermi", Rome, Italy

<sup>13</sup> Chicago State University, Chicago, USA

<sup>14</sup> Commissariat à l'Energie Atomique, IRFU, Saclay, France

<sup>15</sup> COMSATS Institute of Information Technology (CIIT), Islamabad, Pakistan

<sup>16</sup> Departamento de Física de Partículas and IGFAE, Universidad de Santiago de Compostela, Santiago de Compostela, Spain

<sup>17</sup> Department of Physics and Technology, University of Bergen, Bergen, Norway

<sup>18</sup> Department of Physics, Aligarh Muslim University, Aligarh, India

<sup>19</sup> Department of Physics, Ohio State University, Columbus, OH, USA

<sup>20</sup> Department of Physics, Sejong University, Seoul, South Korea

<sup>21</sup> Department of Physics, University of Oslo, Oslo, Norway

<sup>22</sup> Dipartimento di Fisica dell'Università 'La Sapienza' and Sezione INFN, Rome, Italy

<sup>23</sup> Dipartimento di Fisica dell'Università and Sezione INFN, Cagliari, Italy

<sup>24</sup> Dipartimento di Fisica dell'Università and Sezione INFN, Trieste, Italy

<sup>25</sup> Dipartimento di Fisica dell'Università and Sezione INFN, Turin, Italy

<sup>26</sup> Dipartimento di Fisica e Astronomia dell'Università and Sezione INFN, Bologna, Italy

<sup>27</sup> Dipartimento di Fisica e Astronomia dell'Università and Sezione INFN, Catania, Italy

- 28 Dipartimento di Fisica e Astronomia dell'Università and Sezione INFN, Padua, Italy
- 29 Dipartimento di Fisica 'E.R. Caianiello' dell'Università and Gruppo Collegato INFN, Salerno, Italy
- 30 Dipartimento di Scienze e Innovazione Tecnologica dell'Università del Piemonte Orientale and Gruppo Collegato INFN, Alessandria, Italy
- 31 Dipartimento Interateneo di Fisica 'M. Merlin' and Sezione INFN, Bari, Italy
- 32 Division of Experimental High Energy Physics, University of Lund, Lund, Sweden
- 33 Eberhard Karls Universität Tübingen, Tübingen, Germany
- 34 European Organization for Nuclear Research (CERN), Geneva, Switzerland
- 35 Faculty of Engineering, Bergen University College, Bergen, Norway
- 36 Faculty of Mathematics, Physics and Informatics, Comenius University, Bratislava, Slovakia
- 37 Faculty of Nuclear Sciences and Physical Engineering, Czech Technical University in Prague, Prague, Czech Republic
- 38 Faculty of Science, P.J. Šafárik University, Kosice, Slovakia
- 39 Frankfurt Institute for Advanced Studies, Johann Wolfgang Goethe-Universität Frankfurt, Frankfurt, Germany
- 40 Gangneung-Wonju National University, Gangneung, South Korea
- 41 Department of Physics, Gauhati University, Guwahati, India
- 42 Helsinki Institute of Physics (HIP), Helsinki, Finland
- 43 Hiroshima University, Hiroshima, Japan
- 44 Indian Institute of Technology Bombay (IIT), Mumbai, India
- 45 Indian Institute of Technology Indore (IITI), Indore, India
- 46 Inha University, Incheon, South Korea
- 47 Institut de Physique Nucléaire d'Orsay (IPNO), Université Paris-Sud, CNRS-IN2P3, Orsay, France
- 48 Institut für Informatik, Johann Wolfgang Goethe-Universität Frankfurt, Frankfurt, Germany
- 49 Institut für Kernphysik, Johann Wolfgang Goethe-Universität Frankfurt, Frankfurt, Germany
- 50 Institut für Kernphysik, Westfälische Wilhelms-Universität Münster, Münster, Germany
- 51 Institut Pluridisciplinaire Hubert Curien (IPHC), Université de Strasbourg, CNRS-IN2P3, Strasbourg, France
- 52 Institute for Nuclear Research, Academy of Sciences, Moscow, Russia
- 53 Institute for Subatomic Physics of Utrecht University, Utrecht, The Netherlands
- 54 Institute for Theoretical and Experimental Physics, Moscow, Russia
- 55 Institute of Experimental Physics, Slovak Academy of Sciences, Kosice, Slovakia
- 56 Institute of Physics, Academy of Sciences of the Czech Republic, Prague, Czech Republic
- 57 Institute of Physics, Bhubaneswar, India
- 58 Institute of Space Science (ISS), Bucharest, Romania
- 59 Instituto de Ciencias Nucleares, Universidad Nacional Autónoma de México, Mexico City, Mexico
- 60 Instituto de Física, Universidad Nacional Autónoma de México, Mexico City, Mexico
- 61 iThemba LABS, National Research Foundation, Somerset West, South Africa
- 62 Joint Institute for Nuclear Research (JINR), Dubna, Russia
- 63 Konkuk University, Seoul, South Korea
- 64 Korea Institute of Science and Technology Information, Taejeon, South Korea
- 65 KTO Karatay University, Konya, Turkey
- 66 Laboratoire de Physique Corpusculaire (LPC), Clermont Université, Université Blaise Pascal, CNRS-IN2P3, Clermont-Ferrand, France
- 67 Laboratoire de Physique Subatomique et de Cosmologie, Université Grenoble-Alpes, CNRS-IN2P3, Grenoble, France
- 68 Laboratori Nazionali di Frascati, INFN, Frascati, Italy
- 69 Laboratori Nazionali di Legnaro, INFN, Legnaro, Italy
- 70 Lawrence Berkeley National Laboratory, Berkeley, CA, USA
- 71 Lawrence Livermore National Laboratory, Livermore, CA, USA
- 72 Moscow Engineering Physics Institute, Moscow, Russia
- 73 National Centre for Nuclear Studies, Warsaw, Poland
- 74 National Institute for Physics and Nuclear Engineering, Bucharest, Romania
- 75 National Institute of Science Education and Research, Bhubaneswar, India
- 76 Niels Bohr Institute, University of Copenhagen, Copenhagen, Denmark
- 77 Nikhef, National Institute for Subatomic Physics, Amsterdam, The Netherlands
- 78 Nuclear Physics Group, STFC Daresbury Laboratory, Daresbury, UK

- <sup>79</sup> Nuclear Physics Institute, Academy of Sciences of the Czech Republic, Řež u Prahy, Czech Republic
- <sup>80</sup> Oak Ridge National Laboratory, Oak Ridge, TN, USA
- <sup>81</sup> Petersburg Nuclear Physics Institute, Gatchina, Russia
- <sup>82</sup> Physics Department, Creighton University, Omaha, NE, USA
- <sup>83</sup> Physics Department, Panjab University, Chandigarh, India
- <sup>84</sup> Physics Department, University of Athens, Athens, Greece
- <sup>85</sup> Physics Department, University of Cape Town, Cape Town, South Africa
- <sup>86</sup> Physics Department, University of Jammu, Jammu, India
- <sup>87</sup> Physics Department, University of Rajasthan, Jaipur, India
- <sup>88</sup> Physik Department, Technische Universität München, Munich, Germany
- <sup>89</sup> Physikalisches Institut, Ruprecht-Karls-Universität Heidelberg, Heidelberg, Germany
- <sup>90</sup> Politecnico di Torino, Turin, Italy
- <sup>91</sup> Purdue University, West Lafayette, IN, USA
- <sup>92</sup> Pusan National University, Pusan, South Korea
- <sup>93</sup> Research Division and ExtreMe Matter Institute EMMI, GSI Helmholtzzentrum für Schwerionenforschung, Darmstadt, Germany
- <sup>94</sup> Rudjer Bošković Institute, Zagreb, Croatia
- <sup>95</sup> Russian Federal Nuclear Center (VNIIEF), Sarov, Russia
- <sup>96</sup> Russian Research Centre Kurchatov Institute, Moscow, Russia
- <sup>97</sup> Saha Institute of Nuclear Physics, Kolkata, India
- <sup>98</sup> School of Physics and Astronomy, University of Birmingham, Birmingham, UK
- <sup>99</sup> Sección Física, Departamento de Ciencias, Pontificia Universidad Católica del Perú, Lima, Peru
- <sup>100</sup> Sezione INFN, Bari, Italy
- <sup>101</sup> Sezione INFN, Bologna, Italy
- <sup>102</sup> Sezione INFN, Cagliari, Italy
- <sup>103</sup> Sezione INFN, Catania, Italy
- <sup>104</sup> Sezione INFN, Padua, Italy
- <sup>105</sup> Sezione INFN, Rome, Italy
- <sup>106</sup> Sezione INFN, Trieste, Italy
- <sup>107</sup> Sezione INFN, Turin, Italy
- <sup>108</sup> SSC IHEP of NRC Kurchatov institute, Protvino, Russia
- <sup>109</sup> SUBATECH, Ecole des Mines de Nantes, Université de Nantes, CNRS-IN2P3, Nantes, France
- <sup>110</sup> Suranaree University of Technology, Nakhon Ratchasima, Thailand
- <sup>111</sup> Technical University of Split FESB, Split, Croatia
- <sup>112</sup> The Henryk Niewodniczanski Institute of Nuclear Physics, Polish Academy of Sciences, Kraków, Poland
- <sup>113</sup> Physics Department, The University of Texas at Austin, Austin, TX, USA
- <sup>114</sup> Universidad Autónoma de Sinaloa, Culiacán, Mexico
- <sup>115</sup> Universidade de São Paulo (USP), São Paulo, Brazil
- <sup>116</sup> Universidade Estadual de Campinas (UNICAMP), Campinas, Brazil
- <sup>117</sup> University of Houston, Houston, TX, USA
- <sup>118</sup> University of Jyväskylä, Jyväskylä, Finland
- <sup>119</sup> University of Liverpool, Liverpool, UK
- <sup>120</sup> University of Tennessee, Knoxville, TN, USA
- <sup>121</sup> University of Tokyo, Tokyo, Japan
- <sup>122</sup> University of Tsukuba, Tsukuba, Japan
- <sup>123</sup> University of Zagreb, Zagreb, Croatia
- <sup>124</sup> Université de Lyon, Université Lyon 1, CNRS/IN2P3, IPN-Lyon, Villeurbanne, France
- <sup>125</sup> V. Fock Institute for Physics, St. Petersburg State University, St. Petersburg, Russia
- <sup>126</sup> Variable Energy Cyclotron Centre, Kolkata, India
- <sup>127</sup> Vestfold University College, Tonsberg, Norway
- <sup>128</sup> Warsaw University of Technology, Warsaw, Poland
- <sup>129</sup> Wayne State University, Detroit, MI, USA
- <sup>130</sup> Wigner Research Centre for Physics, Hungarian Academy of Sciences, Budapest, Hungary



<sup>131</sup> Yale University, New Haven, CT, USA

<sup>132</sup> Yonsei University, Seoul, South Korea

<sup>133</sup> Zentrum für Technologietransfer und Telekommunikation (ZTT), Fachhochschule Worms, Worms, Germany

<sup>a</sup> Deceased

<sup>b</sup> Also at: St. Petersburg State Polytechnical, St. Petersburg, Russia, University

<sup>c</sup> Also at: Department of Applied Physics, Aligarh Muslim University, Aligarh, India

<sup>d</sup> Also at: M.V. Lomonosov Moscow State University, D.V. Skobeltsyn Institute of Nuclear Physics, Moscow, Russia

<sup>e</sup> Also at: University of Belgrade, Faculty of Physics and “Vinča” Institute of Nuclear Sciences, Belgrade, Serbia

<sup>f</sup> Permanent Address: Konkuk University, Seoul, Korea

<sup>g</sup> Also at: Institute of Theoretical Physics, University of Wrocław, Wrocław, Poland

<sup>h</sup> Also at: University of Kansas, Lawrence, KS, USA